Eur. Phys. J. B (2012) 85: 204
DOI: 10.1140/epjb/e2012-21039-x

THE EUROPEAN PHYSICAL JOURNAL B

Regular Article

DFT study of noble metal impurities on TiO_2(110)

E. Mete[1,a], O. Gülseren[2], and Ş. Ellialtıoğlu[3]

[1] Department of Physics, Balıkesir University, 10145 Balıkesir, Turkey
[2] Department of Physics, Bilkent University, 06800 Ankara, Turkey
[3] Department of Physics, Middle East Technical University, 06800 Ankara, Turkey

Received 16 December 2011 / Received in final form 20 February 2012
Published online 20 June 2012 – © EDP Sciences, Società Italiana di Fisica, Springer-Verlag 2012

Abstract. Atomic and electronic structures of TiO_2(110) surface with possible adsorptional, substitutional and interstitial Au or Pt elemental impurities at full and one-sixth monolayer concentrations were investigated by density functional theory calculations using the projector augmented wave approach within the plane wave method. Relative thermodynamic stabilities of such phases have been discussed by means of their surface free energies. Our results suggest that tunable photocatalytic activity can be achieved on Pt atom admixed rutile (110) surface at low coverages.

1 Introduction

Titanium dioxide (TiO_2) attracts an increased interest as a catalyst support. Gold nanoparticles on titania were shown to exhibit remarkable catalytic activity [1]. Another important metal-on-oxide system is platinum incorporated TiO_2 which finds applications as catalysts and gas sensors [2]. Pt/TiO_2 system has drawn further attention because of its photocatalytic activity towards water decomposition [3]. In recent studies, these noble metals supported on TiO_2 has shown to perform highly efficient catalysis under solar light irradiation [4–7].

As a wide-gap semiconductor, the rutile TiO_2(110) surface is considered to be the generic model system for oxide surfaces. The (110) surface of rutile structure has the lowest surface energy among the other facets [8–12]. It is reducible by surface oxygen vacancy creation or metal incorporation which attracts a great deal of interest for fundamental study of photo- and heterogeneous catalysis [13–16], functional ultrathin films [17,18] and dielectrics [19,20]. Understanding of the properties of metal-metal oxide interface can provide important insights into the applications of real catalysts.

Bonding of gold on titania has been studied to shed light on the effect of Au-substrate adhesion on its catalytic behaviour both experimentally [21–27] and theoretically [28–41]. Similarly, the adsorption properties of Pt have also been investigated by many experiments [3,42–47] and by a few theoretical studies [32,33,48,49]. Although the noble metal-enhanced catalytic activity of rutile TiO_2 has been reported by experiments, the electronic properties of such systems as the originating factor are still not well known.

[a] e-mail: emete@balikesir.edu.tr

Moreover, the incorporation of noble metals like Au and Pt to TiO_2 substrate can be interstitial or substitutional as well as being adsorptional. Indeed, experiments showed that Pt atoms can thermally diffuse into TiO_2 lattice under oxidising atmosphere [50]. Futhermore, these diffused Pt atoms can substitute Ti^{4+} when oxidised to Pt^{2+} or they form interstitials inside. Such metal impurities are known to greatly influence the electronic and catalytic properties of the combined system.

In this paper, we studied the structural and electronic properties of adsorptional, substitutional, and interstitial Au or Pt impurities on rutile TiO_2(110) surface at high (1 ML) and at low (1/6 ML) concentrations. Relative thermodynamic stabilities of such impurity phases have also been discussed. Our primary aim is to elucidate the effect of Au(Pt) incorporation on the electronic structure of the titania substrate at the fundamental level. In this sense, we give emphasis on the electronic behaviour – as well as on the photocatalytic activity – as a result of the bonding characteristics of such an incorporation rather than investigating the formation of such impurities.

2 Method

The calculations have been performed by the density functional theory (DFT) implementation of the VASP [51] code. Exchange-correlation energy has been approximated by the gradient corrected Perdew-Burke-Ernzerhof (PBE96) functional [52]. We used projector augmented waves (PAW) approach [53,54] with a plane-wave basis up to a cutoff of 400 eV.

We considered the bulk terminated (1×1) and (3×2) supercells as the slab models for high (1 ML) and

low (1/6 ML) metal coverages, respectively. Bulk terminated rutile TiO_2(110)-(1×1) and TiO_2(110)-(3×2) surfaces have been modeled by a symmetric slab of 7 TiO_2 trilayers separated by ∼15 Å of vacuum region. Each trilayer consists of a central O–Ti–O plane and 2 oxygen atoms placed symmetrically above and below this plane.

For the geometry optimisation calculations, the Brillouin Zones of (1×1) and (3×2) supercells were sampled with a 8×5×1 and 2×2×1 k-point meshes, respectively. In all calculations, the full relaxation has been performed using conjugate-gradient algorithm based on the reduction of the Hellmann-nFeynman forces on each atom to less than 0.01 eV Å^{-1}. Density of states (DOS) calculations were performed on 16×12×1 and 6×6×1 grids for the (1×1) and (3×2) surface unit cells, respectively.

We calculated the binding energy of adsorbate, M, by

$$E_b = (E_{\mathrm{M/TiO_2}} - E_{\mathrm{TiO_2}} - 2E_{\mathrm{M}})/2 \quad (1)$$

where $E_{\mathrm{M/TiO_2}}$ is the total energy of the computation cell involving the slab and the atomic impurities, M, $E_{\mathrm{TiO_2}}$ is that of the defect-free stoichiometric slab, and E_{M} is the energy of an isolated M (Au, Pt) atom calculated in its electronic ground state. The factor of 2 in front of E_{M} is because there are two atomic impurities at the top and the bottom of the slab models. Division by 2 in equations (1) and (2) come from the two surfaces of the symmetric slab.

The formation energies of defects in the form of metal atom impurities on (1×1) and (3×2) surfaces has been calculated (as previously described in detail [55,56]) by

$$E_f = (E_{\mathrm{M/TiO_2}} - E_{\mathrm{TiO_2}} - \Delta m\,\mu_{\mathrm{M}} + \Delta n\,\mu_{\mathrm{Ti}})/2A \quad (2)$$

where Δm and Δn are the differences in the number of adsorbate M atoms and surface Ti atoms from the reference stoichiometric TiO_2 slab, respectively. The chemical potentials, μ_{M}, were taken from their reference bulk values of −3.270 eV for Au and of −6.017 eV for Pt, representing their most stable solid phases accessible. In other words, we assume that the surface is in thermodynamic equilibrium with ccp bulk Au or Pt. By the same token, the surface layer must be in equilibrium with the rutile TiO_2 bulk which it comes into contact with. This physical requirement implies $\mu_{\mathrm{Ti}} + 2\mu_{\mathrm{O}} = \mu_{\mathrm{TiO_2}}$, restricting μ_{Ti} within an interval of allowed values. Chemical potential of Ti can be as high as that of its bulk which defines an upper boundary referring to Ti-rich conditions. On the other hand, molecular oxygen defines the most stable phase for μ_{O} so that $\mu_{\mathrm{O}} = \frac{1}{2}E_{\mathrm{O_2}}$ referring to O-rich conditions. This choice, therefore, defines the minimum value of μ_{Ti} through the thermodynamic equilibrium condition, $\mu_{\mathrm{Ti}} + 2\mu_{\mathrm{O}} = \mu_{\mathrm{TiO_2}}$.

3 Results and discussion

Rutile TiO_2 has a direct band gap of 3.03 eV [57] at Γ and it has a UV optical response. Our calculated value is 1.85 eV because of the well known underestimation of GGA functionals due to insufficient cancellation of the self-interaction energy. The band gap can greatly be corrected by employing many-body perturbative corrections up to first order in the screened Coulomb potential, W, known as the GW approximation. A better description of both electronic and optical spectra can be obtained by applying Bethe-Salpeter equation (BSE) including excitonic effects. Such a quasiparticle treatment for the correlation energy starting from the DFT spectrum (Kohn-Sham eigenvalues and wavefunctions) of TiO_2 bulk material has been reported to give scissors-like correction to unoccupied states without noticeable change in the band dispersions [58,59]. Therefore, descriptions of electronic properties based on pure DFT results can be made as far as the band structures are concerned. Furthermore, many-body perturbative approach for a supercell consisting of TiO_2(110)–(3×2) slab with 7 trilayers and a vacuum region of ∼15 Å is computationally very expensive at the GW level [60].

Another important factor is that the surface energy tends to converge with increasing number of trilayers with an odd-even oscillation similar to those reported previously [61–67]. After testing the convergence of surface energetics as a function of the slab thickness we have chosen the seven trilayer model as a compromise between the accuracy and the computational cost. Our calculated value of formation energy for the clean (110) surface is 0.46 J m^{-2} in agreement with recent calculations [68].

The present work not only uses a larger cell (e.g. 252 atoms for (3×2) cell) compared to the previous studies but also puts forward the electronic band structures of TiO_2(110) surface with Au(Pt) atomic impurities at 1 and 1/6 ML coverages. This allows us to discuss the effects of such a metal incorporation on the electronic structures specifically in the gap region to get a better understanding.

3.1 Au(Pt)/TiO_2(110)-(1 × 1)

At 1 ML coverage, Au binds to fivefold coordinated surface Ti (Ti5c) with a bond length of 3.10 Å ($d_{\mathrm{Au-Ti}}$ in Tab. 1) tilted by 14° toward the nearest-neighbor (nn) bridging oxygen (O2c) as shown in Figure 1. Well-ordered Au monolayers where gold being atop Ti5c on (1×1) surface has also been verified by several experiments [22,25,30]. Single Au adsorbates are separated from each other by 2.96 Å along [001] direction. Our calculated gas phase Au dimer length is 2.53 Å in agreement with Hakkinen et al.'s theoretical result of 2.54 Å [69]. Hence, Au adatoms on (1×1) surface form linear metallic chains parallel to the oxygen rows where the interatomic distances are slightly longer than the gold dimer length. This indicates a strong Au–Au coordination. Projected DOS analysis shows that the peak corresponding to the half filled gap state is mainly due to an Au 6s electron. It exhibits high dispersion along X–M and X′–Γ–M reflecting the strength of the bonding along 1D gold chain. It couples to the conduction band (CB) of TiO_2 and is almost flat between Γ and X (reciprocal to [1$\bar{1}$0] direction) indicating a weak adsorption. Yang et al. found the binding energy of 1 ML Au on the relaxed TiO_2(110) to be 1.49 eV at Ti5c site with a Au–Ti

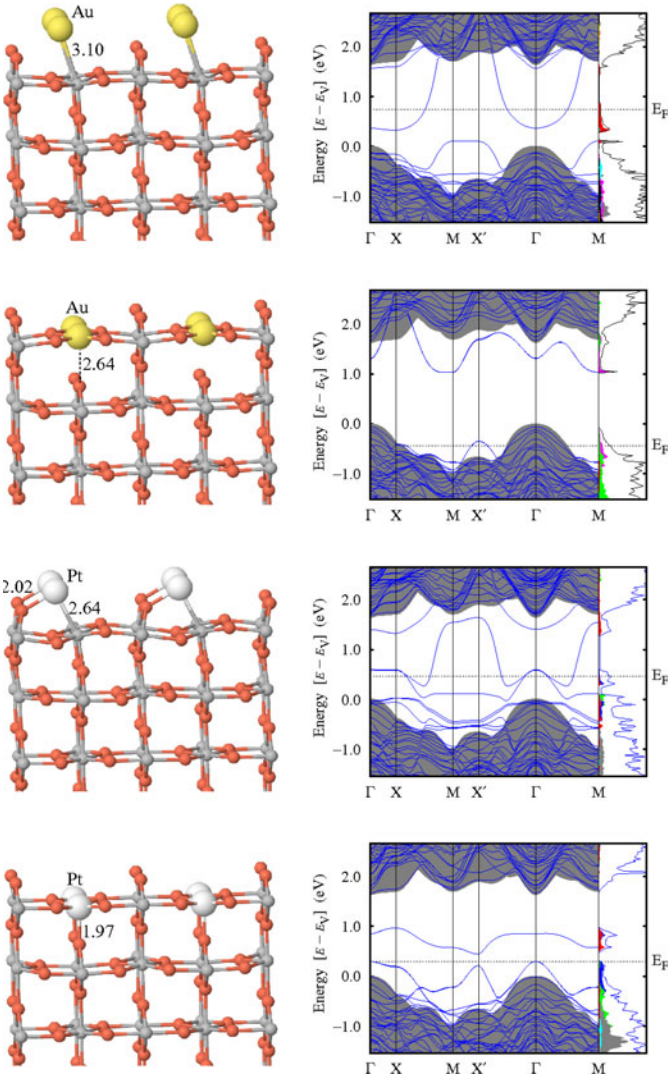

Fig. 1. (Color online) Relaxed geometries (top three trilayers) of the Au(Pt)/TiO_2(110)-(1×1) systems are presented on the left. Their band-gap states along with the corresponding bulk projected band structures (shaded areas) and DOS are shown on the right, next to them. Gray and dark gray (red in color) balls denote Ti and O atoms, respectively. Some key distances between Au(Pt) and (sub)surface atoms are depicted (in Å).

bond length of 2.66 Å through full potential linearised augmented plane-wave (FLAPW) calculations [28]. We calculated the binding energy (BE) of an Au atom on the stoichiometric (1×1) rutile surface to be 1.38 eV. In fact, this BE does not reflect bare metal–substrate interaction, it substantially involves interaction of gold with its periodic images on (1×1) cell causing a significant increase in adsorption energy. Indeed, when we calculated the BE on (3×2) surface it reduces to 0.40 eV where Au adatoms are separated from each other by 8.9 Å along [001] and by 13.1 Å along [1$\bar{1}$0]. Therefore, Au weakly binds to the surface. Moreover, calculating the BE's at all possible adsorption sites, we obtained an almost flat potential energy surface similar to that of Iddir et al. [32,33]. This suggests that gold can diffuse in all directions over the surface in agreement with the existing experimental findings [23,24,26].

Table 1. Calculated values for the M/TiO_2(110) systems (M = Au, Pt): work function and Fermi energy relative to bulk valence band top (in eV), as well as M–O and M–Ti distances (in Å) for each model.

Slab	System		Φ	E_F	d_{M-O}	d_{M-Ti}
(1×1)	Clean		7.22	0.00	–	–
	Au	On	6.16	0.76	2.74	3.10
		Subst	7.39	−0.40	1.97	–
	Pt	On	5.00	0.49	2.02	2.64
		Subst	6.78	0.33	1.96	–
(3×2)	Clean		7.26	0.00	–	–
		on	4.97	1.75	2.02	3.59
	Au	Subst	7.56	−0.05	2.03	–
		In	5.69	1.80	2.18	2.75
		On	6.23	0.63	1.96	2.04
	Pt	Subst	7.39	0.03	2.01	–
		In	6.97	0.46	1.99	2.70

Gold substitution for Ti5c at 1 ML causes considerable distortion on the surface morphology and on the electronic structure as shown in the second row of Figure 1. The distance between Ti5c and the oxygen below which it increases from 1.83 Å to 2.64 Å by Au substitution. The metal dopant interacts with four nn threefold coordinated basal oxygens (O3c) much weaker than Ti does. An explanation might be that the valence of Au, $5d^{10}6s^1$, compared to the valence of Ti, $3d^34s^1$, imposes an electron deficiency. As a result, a half filled Au–O3c driven state appear within the VB setting the Fermi energy below the bulk projected VBM of TiO_2. Additionally, an unoccupied impurity state falls in the gap with a coupling to the CB at about X.

The low energy Pt adsorption site is above Ti5c tilted by 24.7° toward the nn O2c similar to single Au adsorption case but closer to the surface. This site is also referred as the hollow site since it is atop the middle point between two basal oxygens [32,33]. This prediction slightly disagrees with experimental adsorption site atop Ti5c, probably due to a difference in the theoretically predicted and experimentally measured amounts of charge transfer from Pt to TiO_2 [43]. Pt adatom causes noticeable lattice distortions up to the second trilayer (Fig. 1). Unlike the gold case, Pt adatom interacts strongly with rutile (110) surface giving a BE of 2.79 eV on (1×1) cell. It decreases to 2.17 eV on (3×2) cell. Clearly, this lowering is much smaller than that of the Au adatom case, since the contribution from the interaction of Pt with its periodic images is smaller. This is because of the fact that Pt–Pt separation along [001] on (1×1) surface is considerably larger than the Pt dimer length of 2.33 Å due to the lattice parameter (c = 2.96 Å) of the bulk TiO_2. Moreover, Pt ML reduces the work function of the clean surface by 2.22 eV (Tab. 1), more than Au does, due to larger amount of charge transfer from metal to substrate, indicating a stronger binding. Hence, a uniform Pt deposition is relatively more probable than an Au adlayer formation. In

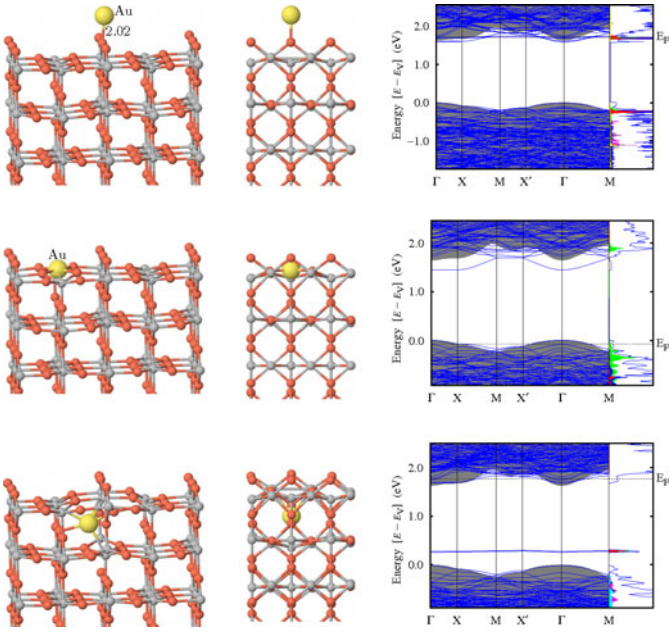

Fig. 2. (Color online) Top three trilayers of fully relaxed Au/TiO_2(110)-(3×2) systems along [1$\bar{1}$0] and [001] directions for adsorptional (on), substitutional (subst) and interstitial (in) cases are shown. Relevant energy band diagrams are presented with DOS (in the rightmost panel) for each of these atomic structures.

fact, Steinrück et al. reported that Pt deposition happens to cause a uniform coverage on the surface at low temperatures (<160 K). Higher substrate temperatures lead to Pt islands by increasing Pt diffusion probability [42]. Pt–O2c and Pt–Ti5c bonds bring two impurity states that disperse strongly across the band gap. Their flat-like dispersion along Γ–X reveals the weakness of Pt–Pt interaction along [1$\bar{1}$0]. Fermi energy crosses these states leading to metallisation. Pt induced distortions, localised to surface layer, bring states at and around the VBM. An upper lying empty impurity state couples to the CB near and between M and X′ modifying its edge.

Substitutional Pt on (1×1) surface does not distort the surface layer as much as an Au dopant does (at the bottom row of Fig. 1). The distance between Pt and subsurface O is 1.97 Å that is slightly extended with respect to Ti–O bond length of 1.83 Å. Having fourfold coordination with basal oxygens, Pt dopant modifies the VB edge by inducing a gap state that elevates the Fermi energy by 0.33 eV at Γ relative to the VBM of the clean surface. Another unoccupied state appears a ∼0.1 eV above the Fermi energy leading to a narrow-gap (indirect between Γ and X′) semiconducting system.

3.2 Au(Pt)/TiO_2(110)-(3 × 2)

The minimum energy adsorption site for single Au on the (3×2) cell with 21 layers has been found to be at above bridging oxygen, O2c, as shown in Figure 2, in agreement with previous theoretical results [26,29,36]. Another preferential site is the the hollow site [31–33,38]. These two configurations do not differ significantly in their total energies and are both experimentally verified [27]. Campbell et al. reported Au monomer adsorption energy to be 0.43 eV by calorimetric measurements [70]. Vijay et al. found that Au binds to an O2c or to a Ti5c atom (with a tilting toward an O2c) weakly by 0.6 eV. We calculated the binding energy of Au on the (3×2) cell to be 0.40 eV which indicates a flat-like potential energy surface. Indeed, the diffusion barriers were found to be so low that Au atoms already diffuse at room temperature (RT) both in the [001] and in the [1$\bar{1}$0] directions [26,32,33,71,72].

On stoichiometric TiO_2(110) surface Au is reported to exhibit a quasi-two-dimensional growth at low concentrations at low temperatures [21,23]. As the deposition rate or temperature increases Au starts to form three dimensional islands. Formation of Au clusters on the surface indicates a very weak metal-substrate interaction. On the other hand, strong binding can be achieved at O2c vacancies. For example, Benz et al. deposited Au atoms on titania surface forming monatomic Au centers [25]. Following experiments by Tong et al. revealed that Au binding can be broken by a hydroxyl group forcing Au out of the adsorption site in the presence of water.

Electronically, single Au adsorbate causes metallisation due to an unpaired 6*s* electron. Moreover, it gives a state just around the CBM and modifies the CB edge. Okazawa et al. determined the work function of TiO_2(110) surface with low gold coverage to be ∼5.3 eV where our value is 4.97 eV. On the other hand, their clean surface value of 5.4 eV is nearly 1.86 eV smaller than ours. The discrepancy can be attributed to possible existence of oxygen vacancies on the sample because such a reduction was shown to cause 2 eV drop in the work function by Vogtenhuber et al. [73]. Our clean surface value rather agrees with theirs of 7.16 eV and also with an experimental result of 6.83 eV as reported in reference [74].

When Au is substituted for an in-plane Ti5c, it distorts nn oxygens similar to (1×1) case, only locally. Furthermore, the overall band structure is very similar too. Due to charge deficiency, Fermi energy falls in the VB of TiO_2 giving rise to metallisation. Clearly, in substitutional cases gold also raises the work function by 0.17 on (1×1) and by 0.30 eV on (3×2) cells due to valence electron deficit.

We found that noble metal atom implantation into TiO_2(110) subsurface interstitial sites at 1 ML concentration is unstable. However, our calculations suggest that metal atoms are possible as interstitials in (3×2) cell, probably at elevated temperatures and/or under oxidising conditions, in agreement with the experimental findings [50,75]. Relevant surface energy diagrams are presented in Figure 4 where the formation of Au in (3×2) phase is about 0.75 eV higher than that of the clean surface. Single Au implanted cell appears to be metallic just like the previous cases. A flat going impurity state lies ∼0.3 eV above the VBM of TiO_2.

Adsorbate-induced modification of the substrate morphology is more pronounced for Pt on rutile (110) relative to the Au case. For instance, Pt pulls nn Ti5c and O2c

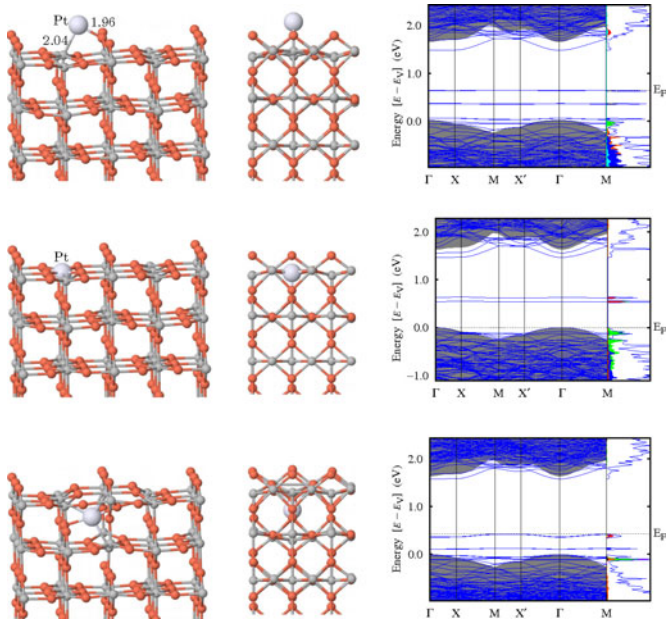

Fig. 3. (Color online) Atomic structures of $Pt/TiO_2(110)$-(3×2) systems along $[1\bar{1}0]$ and [001] directions for adsorptional (on), substitutional (subst) and interstitial (in) cases. Relevant energy band diagrams and DOS are presented on the right for each of them.

toward itself at the expense of extending their bonds with the lattice. This indicates relatively stronger binding with 2.17 eV adsorption energy at the hollow site (see Fig. 3) in agreement with the BE of 2.14 eV reported by Iddir et al. for Pt on (3×2) with 4 trilayers. This site differs with a tilting angle of $\sim27^\circ$ from experimentally assigned adsorption atop Ti5c atom [43]. The disagreement has been addressed to the difference in theoretically predicted and experimentally estimated amounts of charge on Pt.

Substitutional cases are predicted to exhibit thermodynamic stability comparable to the clean surface under O-rich conditions at low concentrations even at very low temperatures. For this case, we made Bader analysis [76] to determine the amount of charge transfer in the presence of substitutional Pt (or Au) in Table 2. Au transfers charge to nn O more than Pt does. When we look at the second nearest neighbors, this time, for instance, charge accumulation on Ti1 is much larger in the presence of Pt dopant. Therefore, data in Table 2 indicate that Au shows relatively more localised charge transfer while Pt has a more extended coordination around the impurity site.

Experiments confirm the enhancement of photocatalytic activity of titania surfaces by platinisation [45,46]. This can be partly explained by the availability of defect driven gap states that increase transition probabilities. For example, the excess charge localised on the Pt adsorbate causes three flat going states in the band gap, which can also be seen from their strong DOS peaks. These states lie at 0.04, 0.35, and 0.63 eV above the VBM at Γ. Moreover, surface states appear near band edges due to local distortions. A significant band gap narrowing of 0.84 eV is predicted resulting from upper lying flat-like occupied state (0.63 eV above VBM)

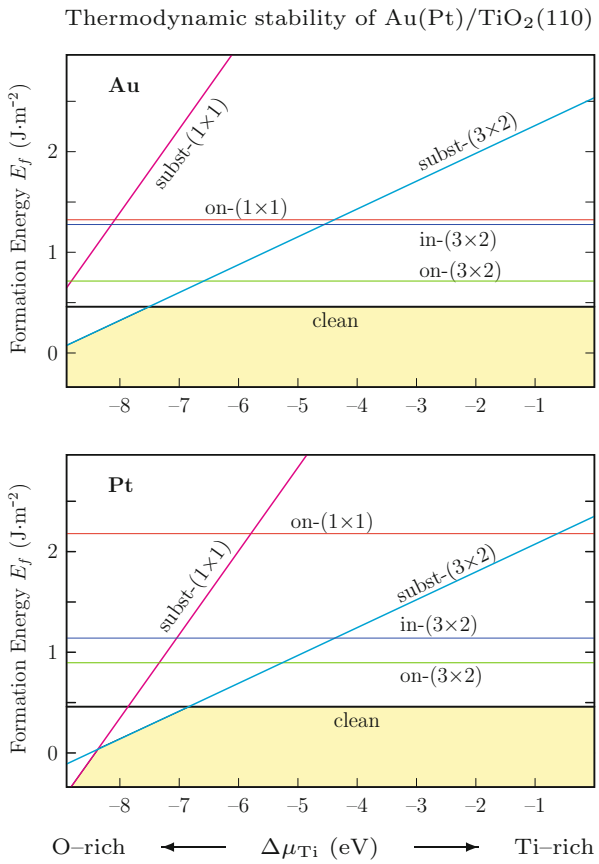

Fig. 4. (Color online) Calculated formation energies of $Au(Pt)/TiO_2(110)$ systems as a function of the chemical potential of Ti.

Table 2. Calculated amount of charges transferred from the metal dopant M (M = Au, Pt) to the neighboring O and Ti sites relative to their clean surface values. O denotes the basal oxygen neighboring to the M atom. Ti1 is the fivefold coordinated surface Ti. Ti2 stands for the bulk-like Ti below the bridging oxygen nearest to the impurity site. ΔQ refers to the total amount of charge transferred from the metal substituent atom to the $TiO_2(110)$ surface.

Slab	Substituent	ΔQ	O	Ti1	Ti2
(1×1)	Au	1.42	–0.366	–	0.009
	Pt	1.74	–0.320	–	0.023
(3×2)	Au	1.28	–0.189	–0.017	–0.013
	Pt	1.68	–0.166	–0.396	0.001

and an unoccupied surface state falling into the gap from the CB (0.21 eV below CBM at Γ).

Relaxation of the clean surface cell causes Ti5c atoms to sink. But, substituted Pt stays levelled with in-plane oxygens (Fig. 3). It slightly pulls the subsurface O3c up. Pt mediates less distortion to the lattice in comparison to the gold case. Moreover, Pt substitution on (3×2) cell is semiconducting whereas a single gold dopant leads to metallisation. In addition, we found that this phase is thermodynamically more stable than the clean surface under oxidising conditions (Fig. 4b). Choi et al. has recently shown that Pt at low doping level significantly enhances

photocatalytic activity of rutile TiO_2 [7]. This must be related to the impurity states. Pt substitute increases the work function by ∼0.13 eV indicating a charge transfer to the lattice that leaves behind empty valence levels on Pt atom. Therefore, Pt substitution on (3×2) cell mainly brings unoccupied gap states, two of which are flat and lie just 0.54 and 0.62 eV above the VBM. A number of bulk-like dispersing impurity driven states fall into the gap from the CB. Together with these states significant effective band gap narrowing leads to the observed increase in photoreactivity.

Zhang et al. reported that Pt can substitute Ti^{4+} under oxidising conditions and can also thermally diffuse into TiO_2 substrate [50]. Therefore, we considered Pt at the interstitial site as shown in the last row of Figure 3. We calculated the formation of such an interstitial phase is ∼0.65 eV relative to that of the bulk terminated surface (Fig. 4b) in line with the experiment. Although it distorts the lattice more than the previous cases, its effect on the energy band structure appears to be comparable to the adsorption phase due to similar bonding characteristics. Pt interstitial brings three occupied states with sharp DOS peaks implying charge localisation around Pt. One of these couples to the VB of the clean surface. Relative to the VBM, the others lie ∼0.12 eV and ∼0.37 eV higher in energy at Γ. They make their minimum at Γ and disperse up to the flat section along M–X′. Fermi energy is set at the top of the upper lying state 0.46 eV above the VBM. As in the case of Pt adsorption, bulk-like surface states fall in the gap from the CB by 0.1 eV at Γ. The resulting band gap narrowing of 0.56 eV corresponds to visible optical response. Such point defects at the interstitial sites might also be important to get a better understanding of the complex behaviour of titania. For instance, in order to offer a possible explanation for the appearance of Ti 3*d* defect state observed on (110) surface reduced by the loss of bridging oxygen(s), Wendt et al. considered an interstitial Ti atom that yields a gap state as observed [75].

4 Conclusions

Au atom binds to the stoichiometric rutile (110) surface much weaker than Pt does. Theory suggests a three dimensional clustering upon gold deposition on the defect-free surface. In this sense, a full Au adlayer is difficult to realise whereas Pt coverage is more probable. Au and Pt diffusion into the (1×1) unit cell is thermodynamically unstable. However, their substitution for Ti5c become even more stable than the clean surface at low concentrations under oxygen rich conditions. Noble metal incorporated phases on (3×2) cell are found to be within the reach of thermal treatment. Therefore, Pt and Au atoms can be adsorbed, or doped as substitutes for the fivefold coordinated Ti atoms, and implanted into interstitial sites in the lattice, at low concentrations. Formation of adsorptional impurities are energetically more favorable than the other two phases.

Both noble metals are expected to promote the catalytic behaviour of TiO_2(110) surface by increasing the reaction probabilities through availability of band-gap states. Stoichiometric TiO_2 gains metallic character upon single Au atom presence due to an unpaired 6*s* electron. Moreover, narrowing of the gap towards visible region results from impurity driven defect states for Pt which, hence, can be used in photocatalysis. The wavelength tuning of photo response of titania might be achieved by different types of Pt incorporation at low coverages.

We acknowledge partial financial support from the Scientific and Technological Research Council of Turkey (TÜBİTAK) (Grant No. 110T394).

References

1. M. Haruta, N. Yamada, T. Kobayashi, S. Iijama, J. Catal. **115**, 301 (1989)
2. V.E. Henrich, P.A. Cox, *The Surface Science of Metal Oxides* (Cambridge Univ. Press, Cambridge, 1994)
3. A. Linsebigler, G. Lu, J.T. Yates Jr., Chem. Rev. **95**, 735 (1995)
4. O.K. Varghese, M. Paulose, T.J. LaTempa, C.A. Grimes, Nano Lett. **9**, 731 (2009)
5. O. Rosseler, M.V. Shankar, M.K.-L. Du, L. Schmidlin, N. Keller, V. Keller, J. Catal. **269**, 179 (2010)
6. S.-Y. Du, Z.-Y. Li, Opt. Lett. **35**, 3402 (2010)
7. J. Choi, H. Park, M.R. Hoffmann, J. Phys. Chem. C **114**, 783 (2010)
8. J. Oviedo, M.J. Gillan, Surf. Sci. **463**, 93 (2000)
9. J. Oviedo, M.J. Gillan, Surf. Sci. **467**, 35 (2000)
10. B. Slater, C.R.A. Catlow, D.H. Gay, D.E. Williams, V. Dusastre, J. Chem. Phys. B **103**, 10644 (1999)
11. F.R. Sensato, R. Custódio, M. Calatayud, A. Beltrán, J. Andrés, J.R. Sambrano, E. Longo, Surf. Sci. **511**, 408 (2002)
12. A. Beltrán, J. Andrés, E. Longo, E.R. Leite, Appl. Phys. Lett. **83**, 635 (2003)
13. M.I. Litter, Appl. Catal. B Env. **23**, 89 (1999)
14. A. Hangfeldt, M. Gratzel, Chem. Rev. **95**, 49 (1995)
15. M. Gratzel, Nature **414**, 338 (2001)
16. S. Khan, J.M. Al-Shahry, W.B. Ingler, Science **297**, 2243 (2002)
17. M. Chen, Y. Cai, Z. Yan, D.W. Goodman, J. Am. Chem. Soc. **128**, 6341 (2006)
18. P. Finetti, F. Sedona, G.A. Rizzi, U. Mick, F. Sutara, M. Svec, V. Matolin, K. Schierbaum, G. Granozzi, J. Phys. Chem. C **111**, 869 (2007)
19. J.M. Wu, C.J. Chen, J. Am. Ceram. Soc. **73**, 420 (1990)
20. G.L. Griffin, K.L. Sieferring, J. Electrochem. Soc. **137**, 1206 (1990)
21. L. Zhang, R. Persaud, T.E. Madey, Phys. Rev. B **56**, 10549 (1997)
22. M.S. Chen, D.W. Goodman, Science **306**, 252 (2004)
23. Y. Maeda, T. Fujitani, S. Tsubota, M. Haruta, Surf. Sci. **562**, 1 (2004)
24. A. Locatelli, T. Pabisiak, A. Pavlovska, T.O. Mentes, L. Aballe, A. Kiejna, E. Bauer, J. Phys.: Condens. Matter **19**, 082202 (2007)
25. L. Benz, X. Tong, P. Kamper, H. Metiu, M.T. Bowers, S.K. Buratto, J. Phys. Chem. B **110**, 663 (2006)

26. D. Matthey, J.G. Wang, S. Wendt, J. Matthiesen, R. Schaub, E. Laegsgaard, B. Hammer, F. Besenbacher, Science **315**, 692 (2007)
27. X. Tong, L. Benz, S. Chretien, H. Metiu, M.T. Bowers, S.K. Buratto, J. Phys. Chem. C **114**, 3987 (2010)
28. Z. Yang, R. Wu, D.W. Goodman, Phys. Rev. B **61**, 14066 (2000)
29. A. Vijay, G. Mills, H. Metiu, J. Chem. Phys. **118**, 6536 (2003)
30. Y. Wang, G.S. Hwang, Surf. Sci. **542**, 72 (2003)
31. D. Pillay, G.S. Hwang, Phys. Rev. B **72**, 205422 (2005)
32. H. Iddir, S. Öğüt, N.D. Browning, M.M. Disco, Phys. Rev. B **72**, R081407 (2005)
33. H. Iddir, S. Öğüt, N.D. Browning, M.M. Disco, Phys. Rev. B **73**, E039902 (2005)
34. D. Pillay, G.S. Hwang, J. Mol. Struc., Theochem **771**, 129 (2006)
35. K. Okazaki-Maeda, Y. Maeda, Y. Morikawa, S. Tanaka, M. Kohyama, Mater. Trans. **47**, 2663 (2006)
36. K. Okazaki-Maeda, Y. Morikawa, S. Ichikawa, S. Tanaka, M. Kohyama, Mater. Trans. **47**, 2669 (2006)
37. T. Okasawa, M. Kohyama, Y. Kido, Surf. Sci. **600**, 4430 (2006)
38. S. Chretian, H. Metiu, J. Chem. Phys. **127**, 084704 (2007)
39. I. Marri, S. Ossicini, Solid State Commun. **147**, 205 (2008)
40. T. Pabisiak, A. Kiejna, Phys. Rev. B **79**, 085411 (2009)
41. F. Yang, M.S. Chen, D.W. Goodman, J. Phys. Chem. C **113**, 254 (2009)
42. H.-P. Steinrück, F. Pesty, L. Zhang, T.E. Madey, Phys. Rev. B **51** 2427 (1995)
43. A. Sasahara, C.L. Pang, H. Onishi, J. Phys. Chem. B **110**, 13453 (2006)
44. A. Sasahara, C.L. Pang, H. Onishi, J. Phys. Chem. B **110**, 17584 (2006)
45. V. Iliev, D. Tomova, L. Bilyarska, A. Eliyas, L. Petrov, Appl. Catal. B Env. **63**, 266 (2006)
46. H. Park, J. Lee, W. Choi, Catal. Today **111**, 259 (2006)
47. N. Isomura, X. Wu, Y. Watanabe, J. Chem. Phys. **131**, 164707 (2009)
48. L. Thien-Nga, T. Paxton, Phys. Rev. B **58**, 13233 (1998)
49. V. Çelik, H. Ünal, E. Mete, Ş. Ellialtıoğlu, Phys. Rev. B **82**, 205113 (2010)
50. M. Zhang, Z. Jin, Z. Zhang, H. Dang, Appl. Surf. Sci. **250**, 29 (2005)
51. G. Kresse, J. Hafner, Phys. Rev. B, **47**, 558 (1993)
52. J.P. Perdew, K. Burke, M. Ernzerhof, Phys. Rev. Lett. **77**, 3865 (1996)
53. P.E. Blöchl, Phys. Rev. B **50**, 17953 (1994)
54. G. Kresse, J. Joubert, Phys. Rev. B **59**, 1758 (1999)
55. E. Mete, D. Uner, O. Gülseren, Ş. Ellialtıoğlu, Phys. Rev. B **79**, 125418 (2009)
56. E. Mete, O. Gülseren, Ş. Ellialtıoğlu, Phys. Rev. B **80**, 035422 (2009)
57. J. Pascaul, J. Camassel, H. Mathieu, Phys. Rev. Lett. **39**, 1490 (1977)
58. L. Chiodo, J.M. García-Lastra, A. Iacomino, S. Ossicini, J. Zhao, H. Petek, A. Rubio, Phys. Rev. B **82**, 045207 (2010)
59. W. Kang, S. Hybertsen, Phys. Rev. B **82**, 085203 (2010)
60. G. Giorgi, M. Palummo, L. Chido, K. Yamashita, Phys. Rev. B **84**, 073404 (2011)
61. M. Ramamoorthy, D. Vanderbilt, R.D. King-Smith, Phys. Rev. B **49**, 16721 (1994)
62. X. Wu, A. Selloni, S.K. Nayak, J. Chem. Phys. **120**, 4512 (2004)
63. T. Bredow, L. Giordano, F. Cinquini, G. Pacchioni, Phys. Rev. B **70**, 035419 (2004)
64. S.J. Thompson, S.P. Lewis, Phys. Rev. B **73** 073403 (2006)
65. K.J. Hameeuw, G. Cantale, D. Ninno, F. Trani, G. Iadonisi, J. Chem. Phys. **124**, 024708 (2006)
66. F. Labat, P. Baranek, C. Adamo, J. Chem. Theory Comput. **4**, 341 (2008)
67. P.M. Kowalski, B. Meyer, D. Marx, Phys. Rev. B **79**, 154410 (2009)
68. A. Hallil, E. Amzallag, S. Landron, R. Tétot, Surf. Sci. **605**, 738 (2011)
69. H. Hakkinen, U. Landman, Phys. Rev. B **62**, R2287 (2000)
70. C.T. Campbell, S.C. Parker, D.E. Starr, Science **298**, 811 (2002)
71. A.S. Wörz, U. Heiz, F. Cinquini, G. Pacchioni, J. Phys. Chem. B **109**, 18418 (2005)
72. A. Del Vitto, G. Pacchioni, F. Delbecq, P. Sautet, J. Phys. Chem. B **109**, 8040 (2005)
73. D. Vogtenhuber, R. Podloucky, J. Redinger, E.L.D. Hebenstreit, W. Hebenstreit, U. Diebold, Phys. Rev. B **65** 125411 (2002)
74. D. Vogtenhuber, R. Podloucky, A. Neckel, S.G. Steinemann, A.J. Freeman, Phys. Rev. B **49**, 2099 (1994)
75. S. Wendt, P.T. Sprunger, E. Lira, G.K.H. Madsen, Z. Li, J.O. Hansen, J. Matthiesen, A. Blekinge-Rasmussen, E. Lagsgaard, B. Hammer, F. Besenbacher, Science **320**, 1755 (2008)
76. W. Tang, E. Sanville, G. Henkelman, J. Phys.: Condens. Matter **21**, 084204 (2009)